Accelerated parameter estimation in Bilby with relative binning

Kruthi Krishna,[1,2] Aditya Vijaykumar,[3,4] Apratim Ganguly,[5,4] Colm Talbot,[6] Sylvia Biscoveanu,[7] Richard N. George,[8] Natalie Williams,[9] and Aaron Zimmerman[8]

[1] *Department of Physics, Indian Institute of Science, Bangalore 560012, India*
[2] *Department of Astrophysics/IMAPP, Faculty of Science, Radboud University, Nijmegen, The Netherlands*
[3] *Canadian Institute for Theoretical Astrophysics, University of Toronto, 60 St George St, Toronto, ON M5S 3H8, Canada*
[4] *International Centre for Theoretical Sciences, Tata Institute of Fundamental Research, Bangalore 560089, India*
[5] *Inter-University Centre for Astronomy and Astrophysics (IUCAA), Post Bag 4, Ganeshkhind, Pune 411 007, India*
[6] *Kavli Institute for Cosmological Physics, The University of Chicago, 5640 South Ellis Avenue, Chicago, Illinois 60637, USA*
[7] *Center for Interdisciplinary Exploration and Research in Astrophysics (CIERA), Northwestern University, 1800 Sherman Ave, Evanston, IL 60201, USA*
[8] *Weinberg Institute, University of Texas at Austin, Austin, TX 78712, USA*
[9] *School of Physics and Astronomy and Institute for Gravitational Wave Astronomy, University of Birmingham, Edgbaston, Birmingham, B15 2TT, United Kingdom*

We describe an implementation of the relative binning technique to speed up parameter estimation of gravitational-wave signals. We first give a pedagogical overview of relative binning, discussing also the expressions for the likelihood marginalized over phase and distance. Then, we describe the details of the code in `Bilby`, an open-source software package commonly used for parameter estimation of gravitational-wave sources. Our code is able to reproduce the parameters of GW170817 in 14 hours on a single-core CPU, performs well on simulated signals, and passes the percentile-percentile (p-p) tests. We also illustrate that relative binning is an ideal technique to estimate the parameters of signals in next-generation gravitational wave detectors.

I. INTRODUCTION

Once a compact binary coalescence (CBC) is detected in data from gravitational wave (GW) detectors such as LIGO [1], Virgo [2], and KAGRA [3–5], it is of interest to understand the properties of the CBC that produced the GWs. These source properties include the masses and spins of the objects in the binary, their distance, orientation and sky location with respect to the detector, etc. Any further downstream analysis makes use of the properties inferred. These downstream analyses could include, for example, inference of the equation of state of neutron stars [6–8], population properties of binary black holes [9, 10], tests of general relativity [11, 12], and parameters of an underlying cosmological model [13]. Therefore, accurate and robust methods of estimating parameters are of utmost importance to GW astronomy. These methods should ideally be quick and computationally efficient—in fact, in certain situations e.g. to permit rapid electromagnetic follow-up of binary neutron star (BNS) mergers or neutron star–black hole (NSBH) mergers, it is desirable to infer the source properties of the neutron stars with a latency of a few minutes.

Bayesian inference is the most favoured methodology for parameter estimation of GW signals. It links a given GW model to the data by constructing posterior distributions for the model parameters. The associated computational cost increases with the dimensionality of the model parameter space and the signal duration. Hence, estimating the source parameters of signals, such as those from BNS events, that last for a long time in ground-based GW detectors is very expensive. Typically, this process takes a few weeks if performed using the most naive Gaussian likelihood prescription. This also does not scale well as we go towards A+ [14, 15] or the next-generation (XG) GW detectors such as Cosmic Explorer [16] and Einstein Telescope [17], as they will have longer in-band signals due to increased sensitivity at lower frequencies and higher detection rate given the overall increase in strain sensitivity.

A number of techniques have been developed to reduce the time it takes to estimate parameters. Most of these techniques either concentrate on accelerating the calculation of likelihood or accelerating the overall sampling process. For instance, the reduced order quadrature (ROQ) method [18–21] speeds up likelihood calculation time by decomposing the waveform parameter space into a set of basis vectors. Since the overlap between the basis vectors can be pre-computed, all that has to be done during sampling is the calculation of the basis coefficients. Other methods of speeding up likelihood computations include multibanded waveform generation [22], multibanded likelihood calculation [23], and the meshfree likelihood approximation [24, 25]. To speed up the sampling process, techniques that rely on parallelized calculations [26–29], non-Markovian methods [30], and machine learning methods [31, 32] also exist. More recently, there have been proposals to implement waveforms in a "auto-differentiable" format to be compatible with `jax` and harness its power to speed up parameter estimation [33, 34].

Relative binning[1] [35–37] is another way of speeding up the likelihood evaluations. It relies on the approximation that the ratio of neighbouring waveforms in the parameter space of GW signals is smooth, and hence can be approximated by a piecewise linear function. This approximation allows the pre-computation of some terms in the likelihood and reduces the number of frequency points at which the waveform needs to be evaluated during sampling, thus enabling parameter estimation of CBCs (especially neutron stars) in a very short amount of time. In this work, we describe the implementation of the relative binning technique in `Bilby` [38, 39], a open-source Bayesian inference package. `Bilby` provides a user-friendly interface for analyzing GW signals and performing accurate and reliable parameter estimation on both real and simulated data alike [38, 39]. We note that there exist other implementations of relative binning [34, 40–42] with varied functionalities, including the generalization to higher harmonics of the GW radiation and precession [43], and optimal coordinate systems for sampling [41, 44]; in what follows, we will restrict our discussion to the implementation of relative binning within `Bilby`, although we shall briefly comment on the validity of our assumptions in Section IV. We also note that an implementation of relative binning compatible with `Bilby` (but not direclty a part of the `Bilby` releases) and including extensions to higher modes and precession for a python implementation of the `IMRPhenomXPHM` waveform is described in Ref. [42].

This paper is structured as follows. In Section II, we provide a pedagogical, technical overview of the relative binning technique. In Section III, we provide details of the implementation of relative binning in `Bilby`. In Section IV, we describe results from consistency tests of our code with both injections and real events alike. Finally, in Section V, we summarize our results and provide a roadmap for future work. The code described is already available in released versions of `Bilby`, and has been used to aid parameter estimation in a number of works (e.g. Refs. [45–49]).

II. TECHNICAL OVERVIEW

The key idea behind relative binning is that waveforms with non-negligible posterior probabilities are alike in the frequency domain and differ only by small perturbations of parameters. A stochastic sampler spends most of its time in a small, high-likelihood neighbourhood around the best-fit waveform. Here the waveforms differ from each other only by small perturbations of parameters (denoted by vector $\boldsymbol{\theta}$), and therefore, the ratio between them will be a smooth function [35–37]. Intuitively, by choosing an appropriate set of breakpoints, any smooth function can be approximated by a piece-wise linear function. Let us try to understand how relative binning uses the knowledge of these breakpoints (bin edges) and piece-wise linear coefficients to downsample the required frequency points. The frequency interval between two consecutive breakpoints constitutes a bin b_i (more on the binning criterion in Section II C). For a given fiducial waveform $\mu_0(f) = \mu(f, \boldsymbol{\theta_0})$, and a close-by waveform, $\mu(f, \boldsymbol{\theta})$, in the high-likelihood neighborhood, the waveform ratio $r(f) = \mu(f)/\mu_0(f)$ can be approximated by

$$r(f) \approx \begin{cases} r_0(b_1) + r_1(b_1)\,(f - f_{\rm m}(b_1))\,, & f \in b_1 \\ r_0(b_2) + r_1(b_2)\,(f - f_{\rm m}(b_2))\,, & f \in b_2 \\ \qquad\vdots \end{cases} \tag{1}$$

where bin $f_m(b_i)$ is the mid-point of the bin b_i. Note that, for each waveform, the coefficients $r_0(b_i)$ and $r_1(b_i)$ are constants in each bin and are independent of frequency. Moreover, due to the linearity assumption, they can be efficiently computed from the values of $r(f)$ at the bin edges. Hence, we have to evaluate $\mu(f, \boldsymbol{\theta})$ only at the bin edges rather than the full frequency array.

A. Summary Data

In the relative binning technique, all the information related to the data and the fiducial waveform is condensed into *summary data* and used as weights for the linear-fit coefficients $r_0(b_i)$ and $r_1(b_i)$ while computing the likelihood. Note that the summary data is independent of the sampled waveform, $\mu(f, \boldsymbol{\theta})$. Therefore, it can be evaluated beforehand; for a given event whose parameters need to be estimated, it only needs to be computed once *before* the sampling commences. In this subsection, we will derive the formulae for summary data, following Ref. [36].

Given the data $d(f)$, the signal duration T, the one-sided noise power spectrum density (PSD) of a detector $S_n(f)$, the complex-overlap [36, 50] between the data and the waveform template is given by

$$Z[d(f), \mu(f,\theta)] = \sum_i \frac{4\; d(f_i)\mu^*(f_i,\theta)}{S_n(f_i)\; T} \tag{2}$$

$$= \sum_{b_j} \left(4 \sum_{f_i \in b_j} \frac{d(f_i)\mu^*(f_i,\theta)}{S_n(f_i)\; T} \right) \quad . \tag{3}$$

Here, x^* denotes the conjugate of x. In the last step above, we summed over the frequency points in each bin first and then took the sum over all the bins. Now let us substitute $\mu^*(f,\theta) = r^*(f)\mu_0^*(f)$ in Eq.(3) and simplify the resulting expression as shown below.

[1] Relative binning is often alternatively referred to as the heterodyned likelihood method at various points in the literature. In the rest of the work, we will continue to use relative binning to refer to this method in order to be consistent with the terminology used in the `Bilby` implementation.

$$
\begin{aligned}
Z[d,\mu] &= \sum_{b_j}\left(4\sum_{f_i\in b_j}\frac{d(f_i)r^*(f_i)\,\mu_0^*(f_i)}{S_n(f_i)\;T}\right)\\
&\approx \sum_{b_j}\Bigg(r_0^*(\mu,b_j)\left(4\sum_{f_i\in b_j}\frac{d(f_i)\;\mu_0^*(f_i)}{S_n(f_i)\;T}\right)\\
&\quad + r_1^*(\mu,b_j)\left(4\sum_{f_i\in b_j}\frac{d(f_i)\;\mu_0^*(f_i)}{S_n(f_i)\;T}(f_i-f_{\rm m}(b_j))\right)\Bigg)\\
&\approx \sum_{b_j}\left(A_0(b_j)r_0^*(\mu,b_j)+A_1(b_j)r_1^*(\mu,b_j)\right) \qquad (4)
\end{aligned}
$$

$$
\begin{aligned}
\text{where}\quad A_0(b_j) &= 4\sum_{f\in b_j}\frac{d(f)\mu_0^*(f)}{S_n(f)\;T}\\
A_1(b_j) &= 4\sum_{f\in b_j}\frac{d(f)\mu_0^*(f)}{S_n(f)\;T}\,(f-f_{\rm m}(b_j))
\end{aligned}
$$

Similarly, we can derive equivalent expressions for $Z[\mu(f),\mu(f)]$. Thereby, we get the following formulae for summary data – $A_0(b_j)$, $A_1(b_j)$, $B_0(b_j)$, $B_1(b_j)$ - and complex-overlaps:

$$
\begin{aligned}
A_0(b_j) &= 4\sum_{f\in b_j}\frac{d(f)\mu_0^*(f)}{S_n(f)\;T}\\
A_1(b_j) &= 4\sum_{f\in b_j}\frac{d(f)\mu_0^*(f)}{S_n(f)\;T}\,(f-f_{\rm m}(b_j))\\
B_0(b_j) &= 4\sum_{f\in b_j}\frac{|\mu_0(f)|^2}{S_n(f)\;T}\\
B_1(b_j) &= 4\sum_{f\in b_j}\frac{|\mu_0(f)|^2}{S_n(f)\;T}\,(f-f_{\rm m}(b_j))
\end{aligned}
\qquad (5)
$$

$$
Z[d(f),\mu(f)] \approx \sum_{b_j}\left(A_0(b_j)r_0^*(\mu,b_j)+A_1(b_j)r_1^*(\mu,b_j)\right) \qquad (6)
$$

$$
\begin{aligned}
Z[\mu(f),\mu(f)] \approx \sum_{b_j}\Big(&B_0(b_j)\,|r_0(\mu,b_j)|^2\\
&+2B_1(b_j)\;\mathfrak{Re}\left[r_0(\mu,b_j)r_1^*(\mu,b_j)\right]\Big) \qquad (7)
\end{aligned}
$$

In Eq. (6) and 7, the complex-overlaps are expressed as functions of terms that are only dependent on the bin, not the frequency itself. Thus, the number of frequency points required to evaluate $Z[d(f),\mu(f)]$ and $Z[\mu(f),\mu(f)]$ is reduced.

For the sake of completeness, we write down the formula used for computing the likelihood below.

$$
\begin{aligned}
\ln\mathcal{L}(\boldsymbol{\theta}) = &\log\mathcal{Z}_{\mathcal{N}} + \;\mathfrak{Re}Z[d(f),\mu(f,\boldsymbol{\theta})]\\
&-\frac{1}{2}Z[\mu(f,\boldsymbol{\theta}),\mu(f,\boldsymbol{\theta})] \qquad (8)
\end{aligned}
$$

Table I. A comparison between quantities evaluated at each frequency point and those only evaluated at bin edges.

Quantity	Evaluated at	
	each f point	**bin edges**
Data (d)	✓	
Fiducial waveform (μ_0)	✓	
A sampled waveform (μ)		✓
Waveform ratio ($r=\mu/\mu_0$)		✓

Table II. Relationship between summary data, linear-fit coefficients, data, fiducial waveform, and sampled waveform.

Quantity	Depends on		
	d	μ_0	μ
Summary data	✓	✓	
linear-fit coefficients r_0 and r_1		✓	✓

where $\mathcal{Z}_{\mathcal{N}}$ is the noise evidence [50]. Tables I and II summarise all the dependencies of various terms we have encountered so far.

B. Phase and Distance Marginalized Likelihoods

In GW parameter estimation, to speed up the calculations and improve convergence, we often explicitly marginalize over extrinsic parameters such as coalescence time, phase (ϕ) [51] and luminosity distance (D_L) [50]. In Appendix A, we argue that marginalizing over coalescence time is not feasible with relative binning. However, the prescription given in Thrane and Talbot [50] for likelihoods marginalized over ϕ and D_L remains the same with relative binning. We rewrite the marginalized likelihoods in complex-overlap notation below:

$$
\begin{aligned}
\log\mathcal{L}^{\phi}_{\rm marg}(\tilde{\boldsymbol{\theta}}) = &\log\mathcal{Z}_N - \frac{1}{2}Z[\mu(\tilde{\boldsymbol{\theta}}),\mu(\tilde{\boldsymbol{\theta}})]\\
&+\log I_0\Big(\Big|Z[d,\mu(\tilde{\boldsymbol{\theta}})]\Big|\Big) \qquad (9)\\
\log\mathcal{L}^{D}_{\rm marg}(\tilde{\boldsymbol{\theta}}) = &\log\mathcal{Z}_N + \log\mathcal{L}_D(\kappa^2(\tilde{\boldsymbol{\theta}}),\rho_{\rm opt}(\tilde{\boldsymbol{\theta}})) \qquad (10)
\end{aligned}
$$

where in each equation, $\tilde{\boldsymbol{\theta}}$ is the set of binary parameters excluding the parameter we are marginalizing over, and I_0 is the modified Bessel function of first kind. The complex overlaps, $\kappa^2 = \mathfrak{Re}(Z[d,\mu])$ and $\rho_{\rm opt} = Z[\mu,\mu]$, are employed in pre-computing a lookup table for $\log\mathcal{L}_D(\kappa^2,\rho_{\rm opt})$ using the integral below.

$$
\begin{aligned}
\mathcal{L}_D(\kappa^2,\rho_{\rm opt}) \equiv \int dD_L\;\exp\Big(&\mathfrak{Re}(Z[d,\mu(\tilde{\boldsymbol{\theta}},D_L)])\\
&-\frac{1}{2}Z[\mu(\tilde{\boldsymbol{\theta}},D_L),\mu(\tilde{\boldsymbol{\theta}},D_L)]\Big)\pi(D_L). \qquad (11)
\end{aligned}
$$

where $\pi(D_L)$ is the prior distribution of D_L.

C. Binning Criterion

Relative binning likelihood is an approximation to the exact likelihood. The likelihood error largely depends on the accuracy of the piece-wise linear approximation of the waveform ratio, $r(f)$. Thus, the objective is to choose a minimal set of breakpoints that fully capture the variations in $r(f)$ and yield a likelihood error within a given tolerance level. We follow Zackay *et al.* [36] in this work. However, an alternate way to do this is outlined in Ref [37].

For small perturbations in parameters, $\Delta\boldsymbol{\theta}$, by expressing a waveform $\mu(f)$, in terms of its phase $\Psi(f)$ and magnitude $|\mu(f)|$, the waveform ratio becomes

$$r(f) = \left|\frac{\mu(f)}{\mu_0(f)}\right| e^{i\Delta_\theta\Psi(f)} \\ \text{where } \Delta_\theta\Psi(f) = \Psi(f, \boldsymbol{\theta_0} + \Delta\boldsymbol{\theta}) - \Psi(f, \boldsymbol{\theta_0}) \tag{12}$$

In the equation above, the magnitude term is slow-varying compared to the phase-difference term, $\Delta_\theta\Psi(f)$. Thus, the oscillations of $r(f)$ are mainly characterized by $\Delta_\theta\Psi(f)$. This allows us to choose the breakpoints based on the criterion that the change in $\Delta_\theta\Psi(f)$ over a frequency bin b_n is some small number ϵ, in radians,

$$\left|\Delta_\theta\Psi(f_{max}(b_n)) - \Delta_\theta\Psi(f_{min}(b_n))\right| = \epsilon. \tag{13}$$

However, note that $\Delta_\theta\Psi(f)$ is dependent on $\boldsymbol{\theta} = \boldsymbol{\theta_0} + \Delta\boldsymbol{\theta}$, which means our breakpoints will be different for each sampled waveform. Let us examine how we can get rid of this $\boldsymbol{\theta}$-dependence in our binning criterion.

In the post-Newtonian theory, $\Psi(f)$ can be formulated as a sum of different powers of f,

$$\Psi(f, \boldsymbol{\theta}) = \sum_k \alpha_k(\boldsymbol{\theta}) f^{\gamma_k}, \tag{14}$$

where α_k's are the power-law coefficients and γ_k's are the power-law indices [52]. The phase-difference $\Delta_\theta\Psi(f)$ does not vary by more than a few cycles for small perturbations $\Delta\boldsymbol{\theta}$. In this case, we can impose a limit on the maximum perturbation of each term in Eq. (14), $|\Delta\alpha_k f^{\gamma_k}|_{max} \approx 2\pi\chi$, where χ is a tunable factor. For a frequency range $[f_{\rm low}, f_{\rm high}]$, this gives us

$$|\Delta\alpha_k^{\rm max}| f_{k_*}^{\gamma_k} \approx 2\pi\chi \\ \text{where } f_{k_*} = \begin{cases} f_{\rm low} & \text{if } \gamma_k < 0 \\ f_{\rm high} & \text{if } \gamma_k > 0 \end{cases} \tag{15}$$

The above equation gives us the maximum perturbation allowed for each α_k in our sampling scenario. Therefore, the phase-difference corresponding to the maximum perturbation of α_k's will be

$$\Delta_\theta\Psi'(f) = \sum_k \Delta\alpha_k^{\rm max}\ f^{\gamma_k} \\ = 2\pi\chi \sum_k \left(\frac{f}{f_{k_*}}\right)^{\gamma_k} \text{sgn}(\gamma_k). \tag{16}$$

In the last step above, the sign function, $\text{sgn}(\gamma_k)$, is added to each term in the summation to allow for a scenario where signs of α_k's conspire to generate the maximum phase difference. We shall use this $\boldsymbol{\theta}$-independent estimate of phase difference in Eq. (13) to obtain our binning criterion:

$$f_{max}(b_n) = \Delta_\theta\Psi'^{-1}(n\epsilon + \Delta_\theta\Psi'(f_{\rm low})) \tag{17}$$

where $n = 1, 2, ...,$ is the bin number and $f_{\rm low}$ is the minimum frequency cut-off of our signal.

D. Pre-sampling

For Bayesian parameter estimation with relative binning, prior to the familiar, stochastic sampling, the following pre-sampling steps are necessary:

1. *Setting up bins*: An efficient way to implement Eq. (17) is to divide the range $[\Delta_\theta\Psi'(f_{\rm low}), \Delta_\theta\Psi'(f_{\rm high})]$ in a grid of spacing ϵ and invert the grid points to obtain $f_{max}(b_n)$.

2. *Fixing the fiducial waveform*: Reasonable choices for fiducial parameters ($\boldsymbol{\theta_0}$) would be the best-fit parameters outputted by matched filter searches, the maximum likelihood parameters or injection parameters in case of an injected signal [36, 53].

3. *Computing summary data*: With the knowledge of the data, fiducial waveform, bins, and the noise PSD, we can obtain the summary data for each detector using Eq. (5).

E. Sampling

Posterior distributions for a chosen set of parameters are obtained by stochastic sampling different waveforms in the parameter space. To evaluate the corresponding likelihood value for each sampled waveform, we execute the following steps:

1. *Evaluate* $\mu(f)$: Here the waveform is generated only for the bin edges rather than the full frequency grid. This immensely reduces the overall waveform generation runtime.

2. *Calculate* $r(f)$: At each bin edge, we calculate the ratio between the sampled waveform $\mu(f)$ and the fiducial waveform $\mu_0(f)$.

3. *Obtain* r_0 *and* r_1: Using the waveform ratio values at the bin edges, the linear-fit coefficients r_0 and r_1 can be obtained for each bin with simple algebra.

4. *Compute the complex-overlaps and the likelihood*: In the final step, we calculate the complex-overlaps and the likelihood using Eqs. (6), (7), and (8).

III. IMPLEMENTATION IN BILBY

Our implementation of the relative binning technique has been publicly available `Bilby` [38] since version 1.4.0. We added a new likelihood subclass called `RelativeBinningGravitationalWaveTransient` which, once setup, internally calls different functions that carry out various steps described in the previous sections. We outline a few important functions below:

- `setup_bins` computes the $\Delta_\theta\Psi'$ for the full frequency array that `waveform_generator` generates using five power-law indices $\gamma_k = \{-5/3, -2/3, 1, 5/3, 7/3\}$ [36] corresponding to the five leading-order post-newtonian terms (see e.g. Ref. [54]), then divides it into a ϵ-spaced grid and inverts those $\Delta_\theta\Psi'-$ grid points to obtain our frequencies bin edges. Thereby, the number of $\Delta_\theta\Psi'-$ grid points determines the total number of bins used in the analysis.

- `set_fiducial_waveforms` evaluates the fiducial waveform values for the full frequency array using the input fiducial parameters. However, if no user-input fiducial parameters are available, a set of parameters is randomly drawn from the prior. We also allow the user to input an initial guess for the fiducial parameters and refine it further using a pre-computed optimization technique by invoking `update_fiducial_parameters=True`. This is done using by running a few iterations of a `scipy.optimize` [55] routine called through a helper function `find_maximum_likelihood_parameters`.

- `compute_summary_data` computes and stores the summary data for each interferometer used.

- `compute_waveform_ratio_per_interferometer` evaluates the waveforms at bin edges and calculates the waveform ratio using the already stored fiducial waveform for each interferometer.

- `calculate_snrs` computes the complex overlaps (equation 6 and 7) for each interferometer, using the summary data and waveform ratios.

Furthermore, we have introduced new source models `lal_binary_neutron_star_relative_binning` and `lal_binary_black_hole_relative_binning` that allow waveform generation at bin edges rather than the full frequency array. However, they can be set to utilize the full frequency array when generating an injected signal[2] by adding an additional parameter `fiducial=1` to the injection parameter dictionary.

[2] An example for performing parameter estimation with relative binning on an injected signal can be found in the `Bilby` git repository at this URL.

We note that, by implementing this likelihood in `Bilby`, we have extended the implementation of relative binning used in Zackay *et al.* [36] to incorporate a fully coherent network statistic and include extrinsic parameters such as distance, sky location, inclination, and polarization (also see [40, 56]), and enabled marginalization over the coalescence phase and luminosity distance as described in subsection II B. Furthermore, in appendix A, we argue that time marginalization is not practical for relative binning in `Bilby`.

IV. RESULTS

In this section, we first compare the performance of relative binning against the exact method in terms of accuracy and computational costs for both real and simulated signals. Then, we explore the accuracy of the current implementation of relative binning for non-quadrupolar waveforms and its use for next-generation detectors. Unless otherwise specified, the priors are uniform in $\sin\delta$ where δ is declination, uniform in $\cos\theta_{JN}$ where θ_{JN} is the orientation angle, and uniform in right ascension α, polarization angle ψ, coalescence phase ϕ_c in their respective ranges. All analyses are performed with v2.1.2 of `Bilby` and v1.1.2 of `Bilby_pipe`. We use the `Dynesty` sampler [57] as implemented in `Bilby` with the custom `acceptance-walk` stepping method (nlive=1000, naccept=60) to sample over relevant parameters.

A. GW170817 Parameter Estimation

BNS events like GW170817 [58] span the entire range of detectable frequencies of LIGO and Virgo detectors and require a fine sampling of parameter space which makes their parameter estimation computationally much more expensive than a typical binary black hole (BBH). To demonstrate the effectiveness of our code in achieving both accuracy and computational efficiency for such events, we analyzed 256s duration of GW170817 strain data from LIGO Livingston, LIGO Hanford, and the Virgo detectors sampled at 4096 Hz. Our analysis covered a frequency range of 20Hz to 2048Hz, and the sampling time was approximately 14 hours with a single CPU core. We expect the sampling time to improve when parallelized over multiple cores, readily doable with `Bilby`. The initial parameter estimates given in Abbott *et al.* [58] were taken as initial guesses for the fiducial parameters but were further updated to the maximum likelihood estimates by setting `update_fiducial_parameters=True`. To set up the bins, we take $\epsilon = 0.25$ radians (or alternatively $\chi = 2$) informed by the discussions in Zackay *et al.* [36], which results in 123 frequency bins with our code. We use the `IMRPhenomPv2_NRTidal` model [59] and the `Dynesty` sampler [57] coupled with `Bilby` for our analysis.

In order to compare our posteriors to the readily avail-

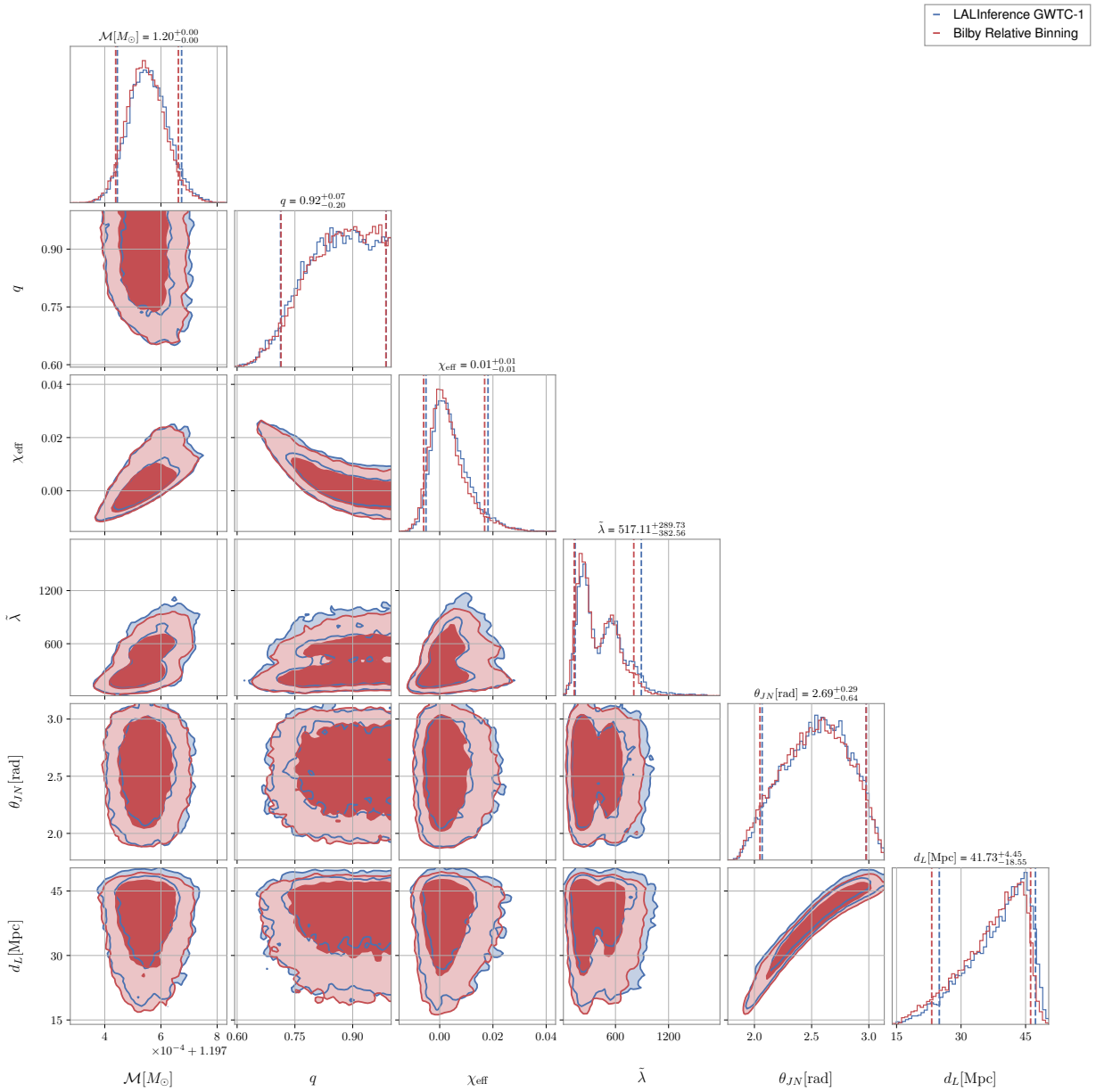

Figure 1. Comparison of posterior distributions from a relative binning parameter estimation of GW170817 in `Bilby` (red) as compared to `LALInference` GWTC-1 samples obtained using the fulllikelihood computation (blue). Marginalized 1-dimensional histograms for each parameter are shown along the diagonal with dashed vertical lines and labels for 5% and 95% quantiles of the parameters. Off-diagonal plots show 2-dimensional joint-posterior distributions with contours corresponding to the 68% and 95% credible regions.

able GWTC-1 [60] samples[3] we have fixed the sky location (right ascension and declination) to the known position of SSS17a/AT 2017gfo as determined by electromagnetic observations [6, 61]. We adopt the low-spin priors, meaning the spin magnitudes of the two neutron stars a_1 and a_2 are drawn uniformly from the interval [0, 0.05]. The priors on mass ratio q is also assumed to be flat between [0.125, 1]. To speed up convergence, we impose a flat prior [1.18, 1.21] $M_\odot$ on the detector frame chirp mass $\mathcal{M}$. We notice that, in general, relative binning performs well when we restrict $\mathcal{M}$ to a small region centred on the fiducial parameter $\mathcal{M}_0$. To be consistent with the prior choices employed in the GWTC-1 result, we reweight the posteriors obtained with a flat prior on chirp mass and mass ratio to a flat prior on the individual component masses. Figure 1 shows a comparison of posteriors between relative binning and

[3] https://dcc.ligo.org/LIGO-P1800370/public

the GWTC-1 samples, which were obtained using the full likelihood calculation. The posteriors obtained from both the methods show excellent agreement with each other. To quantify the "closeness" between the two sets of posterior samples, we use the Jensen-Shannon (JS) divergence [62]. Specifically, we calculate the JS divergence for each parameter that we sampled over, and quote the maximum value of JS divergence across parameters as our similarity statistic. Following Ref. [42], we choose a threshold of 0.06 for the JS divergence. For GW170817, the maximum JS divergence across parameters is 0.007 (corresponding to D_L), well below our threshold.

B. Injection Study

In an injection study, a synthetic GW signal is added to the simulated data and the resulting data stream is analyzed. A brief discussion on how to do this in `Bilby`[4] can be found in Ref. [38]. To assess the performance of our code, we injected non-precessing BBH and BNS signals in typical regions of the parameter space relevant to astrophysical scenarios and performed a full parameter estimation. The injected signals had network SNR ≥ 12. We took the injection parameters to be the fiducial parameters and used 123 frequency bins (ϵ set to 0.25 radians). We repeated the same analysis with the exact method in `Bilby` for the BBH signals. We use the zero noise realization in both cases in order to allow for a one-to-one comparison between the two methods. Here, we used the waveform approximant `IMRPhenomPv2` [63] and sampled all the 15 parameters associated with a BBH merger. Figures 2 and 3 show a comparison of the posteriors from the two methods for an example BBH signal; they agree well with each other, with the maximum JS divergence being 0.004. The injection parameters used in this example are outlined in Table III. The injection was recovered using isotropic priors on spins with spin magnitudes between 0 and 0.99, chirp mass prior uniformly distributed over [20, 60]$M_\odot$, and luminosity distance D_L prior distributed as $\propto D_L^2$ over the range 10 Mpc to 5000 Mpc.

As a full parameter estimation of BNS signals with the exact method takes $\mathcal{O}(10^3)$ core hours, instead of comparing our posteriors with the exact method, we only remark that the injected parameters were well-recovered with respect to their true values. To test this further, we injected 143 BNS signals into simulated Gaussian noise and created a percentile-percentile (p-p) plot [64] of the recoveries. The simulated BNSs were drawn uniformly in chirp mass $\mathcal{M}$ between $1.42M_\odot$ and $1.62M_\odot$, uniformly in mass ratio q between 0.125 and 1, uniformly in individual aligned spin magnitudes χ_1 and χ_2 between -0.05 and 0.05, and uniformly in sky location and orientation of the binary. Luminosity distances for the binaries were drawn assuming a prior $\propto D_L^2$ between 10 Mpc and 300 Mpc. The same priors are used for estimating parameters from these mock signals. For unbiased inference, the p-p plot (shown in Fig. 4) for each of the parameters should lie along the diagonal and should be consistent with error bars coming from finite number of samples. We see that this is the case for all the parameters that we consider, further illustrating that our implementation of relative binning produces unbiased posteriors.

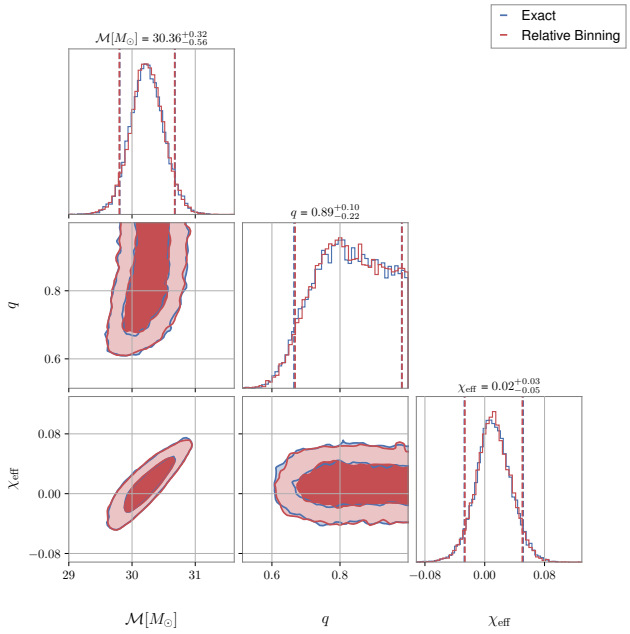

Figure 2. Comparison of posterior distributions for intrinsic parameters of a BBH injection estimated using relative binning (red) and exact (blue) methods in `Bilby`. Marginalized 1-dimensional histograms for each parameter are shown along the diagonal with dashed vertical lines and labels for 5% and 95% quantiles of the parameters. Off-diagonal plots show 2-dimensional joint-posterior distributions with contours corresponding to the 68% and 95% credible regions. The waveform approximant used is `IMRPhenomPv2`.

C. Non-quadrupolar Waveforms

As GWs are a tensor field, they are most naturally decomposed in terms of Y^{-2}_{lm}, the spherical harmonic basis functions of spin-weight -2. For GWs from quasi-circular, non-precessing binaries with comparable masses, waveform templates that consist of only the dominant quadrupole modes ($\ell = 2$, $m = \pm 2$) are sufficient. However, sub-dominant modes play an important role in the detection and parameter estimation of BBHs with high mass ratios or precessing spins. Additionally, the effect of higher harmonics becomes more pronounced as the inclination angle changes from 0 to $\pi/2$ (see e.g. Refs. [65–67]).

[4] An example code can be found here: https://lscsoft.docs.ligo.org/bilby/basics-of-parameter-estimation.html

Table III. Injection parameters used in the results from Section IV B, IV C and IV D.

Parameter	**BBH**	**BBH HM**	**BBH XG**	**BNS XG**
Total detector-frame mass $M_{\rm total}/M_\odot$	70	60	68.92	5.51
Mass Ratio q	0.8	0.5	1	1
Primary spin magnitude a_1	0.01	0.5	0	0
Secondary spin magnitude a_2	0.02	0.5	0	0
Primary spin tilt θ_1	0	1	0	0
Secondary spin tilt θ_2	0	0.5	0	0
Azimuthal angle between the two component spins ϕ_{12}	0	1.7	0	0
Angle between total and orbital angular momenta ϕ_{JL}	0	0.3	0	0
Right ascension α	1.67	2.5	1.67	1.67
Declination δ	-1.26	0	-1.26	-1.26
Geocentric time t_c/s	1126259462	1126259642	1126259462	1126259462
Luminosity Distance D_L/Mpc	701.58	833.54	7000	701.58
Polarization angle ψ	3.93	0	3.9	3.93
Orientation angle θ_{JN}	2.82	1.04	2.82	2.82
Reference phase ϕ	0	0	0	0

Relative binning, as described in Section II, is designed for likelihood evaluations involving only the dominant mode. Using a different set of waveform ratio approximations for each component mode and modified binning schemes, the accuracy of likelihood can be increased for non-quadrupolar waveforms [42, 43].

However, we tested our current implementation on BBHs with $60M_\odot \leq m_{total} \leq 120M_\odot$ and $0.25 \leq q \leq 1$ using the `IMRPhenomXPHM` approximant that includes the effects of non-quadrupole modes $(l, |m|) = (2,2), (2,1), (3,3), (3,2), (4,4)$ and the mode mixing effects in $(l, |m|) = (3,2)$ [68]. We find that the accuracy of posteriors is already quite good despite our code using the simplest prescription of relative binning with 123 frequency bins ($\epsilon = 0.25$). A comparison between the posteriors obtained with relative binning and the exact method for a BBH injection with $m_{total} = 120M_\odot$ and $q = 0.5$ is shown in Figure 5 and 6. The injection parameters are summarized in Table III. The posteriors show good agreement with each other, with the maximum JS divergence being 0.0005 (corresponding to $\mathcal{M}$).

To further test our implementation against signals with significant higher mode content, we perform a parameter estimation of the event GW190412 [69] with relative binning. GW190412 is an asymmetric binary with a mass ratio $q \sim 1/4$, and contains strong evidence for higher order multipoles of GW radiation. We redo the exact-likelihood `Bilby` parameter estimation performed with the `IMRPhenomXPHM` approximant as a part of GWTC-2.1 [70], but with the relative binning likelihood. All choices regarding the prior, sampling frequency, duration etc. are assumed to be exactly the same as that used for generating those samples. To ensure this, we use the C01:IMRPhenomXPHM configurations from the `*_mixed_nocosmo.h5` file corresponding to GW190412 from the GWTC-2.1 Zenodo data release [71] for posterior samples. We also choose our fiducial parameter value as the maximum likelihood sample in the released set of samples. The resulting comparison between samples (for the intrinsic parameters) obtained with the exact likelihood computation and the relative binning likelihood computation is shown in Fig. 7. Again, the posteriors are in good agreement with each other, with a maximum JS divergence of 0.006 (corresponding to the primary spin magnitude a_1). This further showcases the ability of our implementation to recover parameters of signals with higher multipoles even though the prescription is not strictly optimal for such signals.

We leave the `Bilby` implementation of relative binning specific to higher order modes to future work.

D. Relative Binning for XG Detectors

The next-generation (XG) ground-based detectors in the future such as the Einstein Telescope and Cosmic Explorer will have largely improved sensitivity compared to the Advanced LIGO and Virgo detector network. These detectors will have a frequency cutoff as low as f_{low}=5Hz [72]. We will observe currently detectable GW sources with a much higher SNR of the order $\mathcal{O}(10^3)$, thereby, allowing us to study these sources with greater precision [73–75]. However, this would increase the sampling convergence time and make parameter estimation more expensive. Moreover, the inspiral signals can stay in the sensitivity band for a duration ranging between a few hours to days depending on the masses of the binary system [17]. To keep up with such a large amount of data generated, we need faster parameter estimation methods, and relative binning is a promising candidate.

In order to investigate the utility of our code XG de-

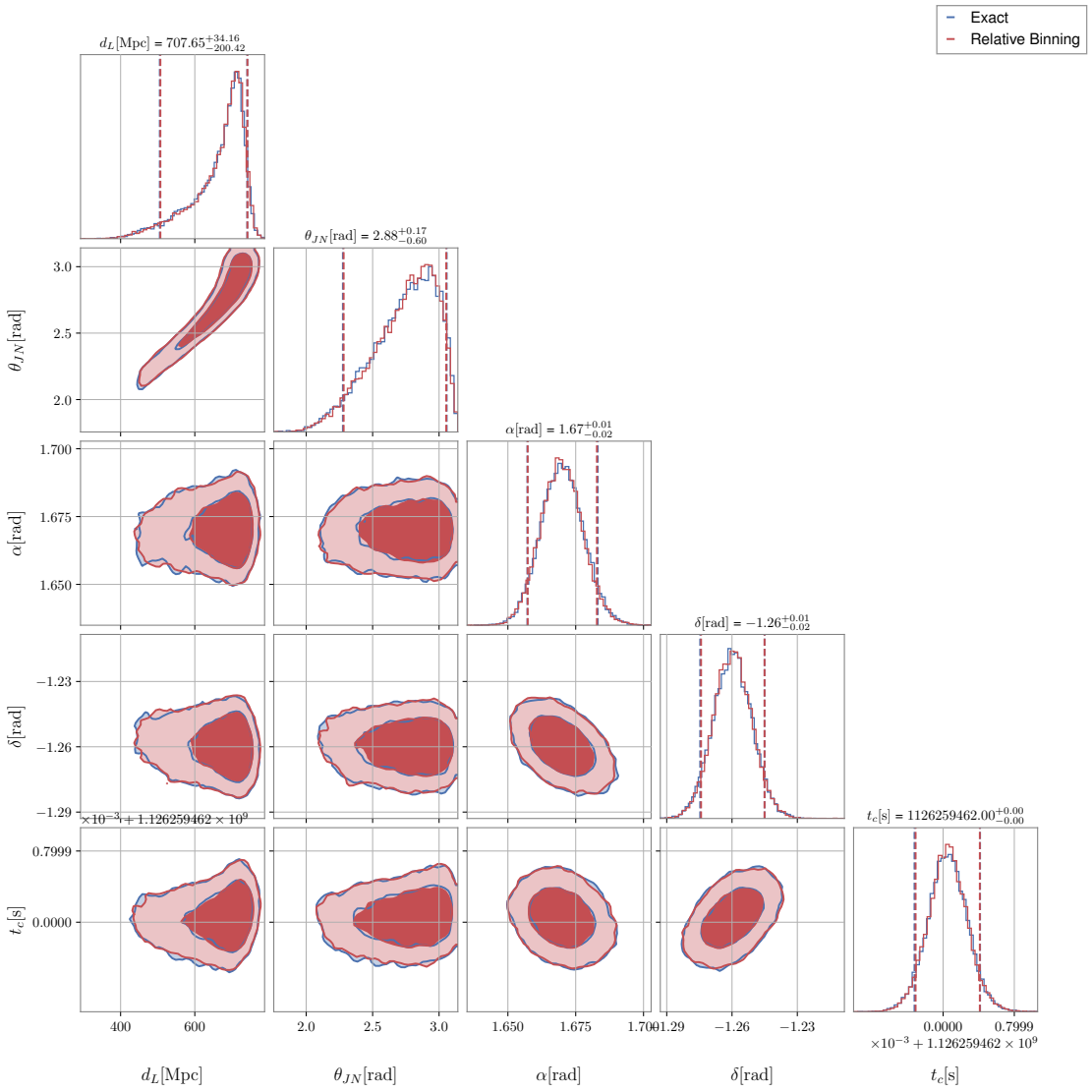

Figure 3. Comparison of posterior distributions for extrinsic parameters of the BBH injection seen in Figure 2, estimated using relative binning (red) and exact (blue) methods in `Bilby`. Marginalized 1-dimensional histograms for each parameter are shown along the diagonal with dashed vertical lines and labels for 5% and 95% quantiles of the parameters. Off-diagonal plots show 2-dimensional joint-posterior distributions with contours corresponding to the 68% and 95% credible regions. The waveform approximant used is `IMRPhenomPv2`.

tections, we injected a BBH and a BNS[5] signal with configurations corresponding to Einstein Telescope (ET) (assumed to be at the location of the Virgo detector in Italy) and Cosmic Explorer (CE) (two equally sensitive detectors at the location of LIGO-Hanford and LIGO-Livingston). For simplicity, we neglect the effect of a time-varying antenna pattern for the BNS injection. The power spectral densities used in this analysis are available[6] in the `detector` module of the `gw` package in `Bilby`. In both cases, the waveform approximant was `IMRPhenomPv2`, and the sampling frequency used was 4096 Hz. For the BBH signal, characterized by a signal duration of 32 seconds and injection parameters as detailed in Table III, the signal-to-noise ratio (SNR) reaches 233, with the associated computational cost totalling to 4 single-core CPU

[5] The configuration used for the BNS signal (equal masses, source frame component mass of 2.4 $M_\odot$) is on the higher side when compared to predictions from standard equations of state of dense matter. While this configuration is probably unrealistic, our main conclusions about the utility of relative binning for XG detectors do not change.

[6] https://git.ligo.org/lscsoft/bilby/tree/master/bilby/gw/detector/noise_curves

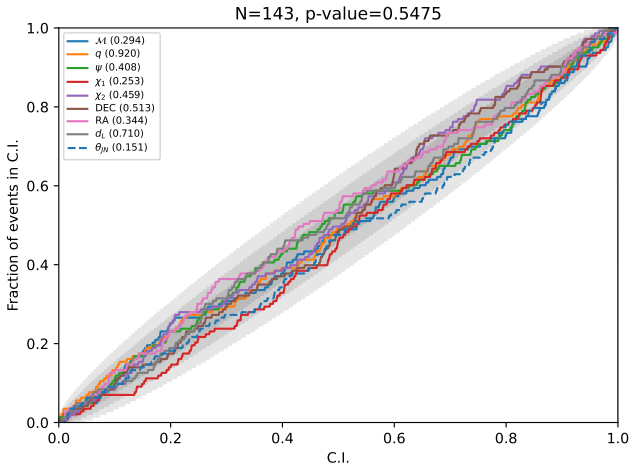

Figure 4. Percentile-percentile (p-p) plot for a set of binary neutron star injections in gaussian noise. For unbiased recovery, the lines should lie perfectly along the diagonal in the above plot. The traces corresponding to all parameter trend along this diagonal, and are consistent with the error regions predicted due to finite number of injections (grey shaded region).

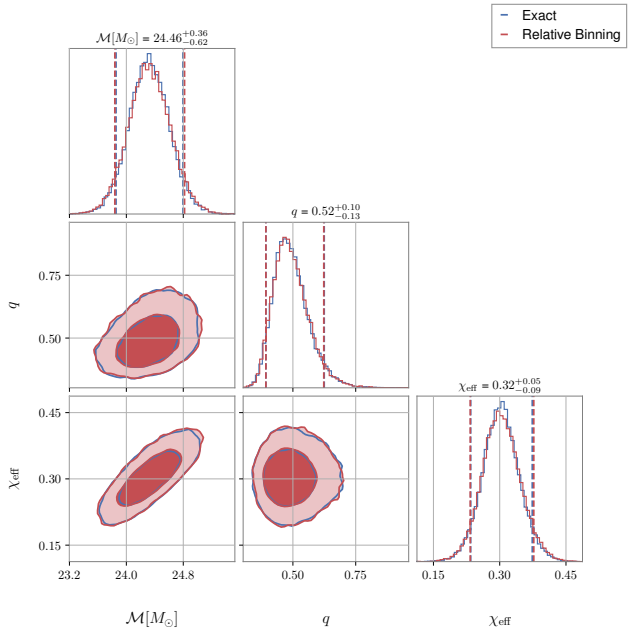

Figure 5. Corner plot comparing the intrinsic parameters estimated using relative binning (red) and exact (blue) methods for a BBH injection with $m_{total} = 120M_\odot$ and $q = 0.5$. The `IMRPhenomXPHM` approximant, which includes the effects of several non-quadrupole modes, was used for likelihood evaluations.

hours. On the other hand, for a BNS signal with a duration of 1024 seconds, a frequency range covering 10 to 2048 Hz, and an SNR of 233, the associated sampling time was 5.5 single-core CPU hours. Table IV summarizes this information. We find that 123 frequency bins are sufficient even in this case.

Table IV. Summary of XG ground-based detector injections

	Signal Duration (seconds)	Frequency Range (Hz)	Sampling Time (core hours)
BBH	32	6-2048	4
BNS	1024	10-2048	5.5

The corner plots of these injections are shown in figures 8, 9, 10 and 11. We see that the posteriors of all the parameters are well-recovered for both signals. The sampling times reported here are comparable to the GW detections with Advanced LIGO/Virgo network despite the huge SNRs. Therefore, relative binning will be tremendously useful for parameter estimation of XG detections.

E. Speed-Up Factors

The speed-up due to relative binning is two-fold. Let us say N is the number of points in a full frequency grid used for parameter estimation with the exact method. For relative binning, the

1. number of points at which a sampled waveform is generated goes as $\mathcal{O}$(number of bins) instead of $\mathcal{O}(N)$.
2. number of overall complex-multiplications involved in likelihood computation goes as $\mathcal{O}$(number of bins) instead of $\mathcal{O}(N)$.

The relative speed-ups are more pronounced when analyzing long chunks of strain data with high sampling rates. For instance, an exact likelihood computation for a binary neutron star merger event like GW170817 with a duration of 256s and a sampling rate of 4096 Hz would require a frequency grid of the order $\sim 10^5$. Whereas, with relative binning, we would only need bins ~ 100. The speed-up factors for different signal lengths are tabulated in Table V. Notice that the time per likelihood evaluation in relative binning is 1-2 milliseconds irrespective of the signal type or duration. This is the case because the number of frequency bins needed to obtain posteriors with the required accuracy remains more or less the same. In all our analyses, we have used only 123 bins. Hence, with an increase in signal duration the speed-up factor scales proportionally.

V. SUMMARY

Parameter estimation of GW signals is a computationally expensive process whose time complexity increases with growing signal durations. Relative binning is a promising candidate for speedy parameter estimation for

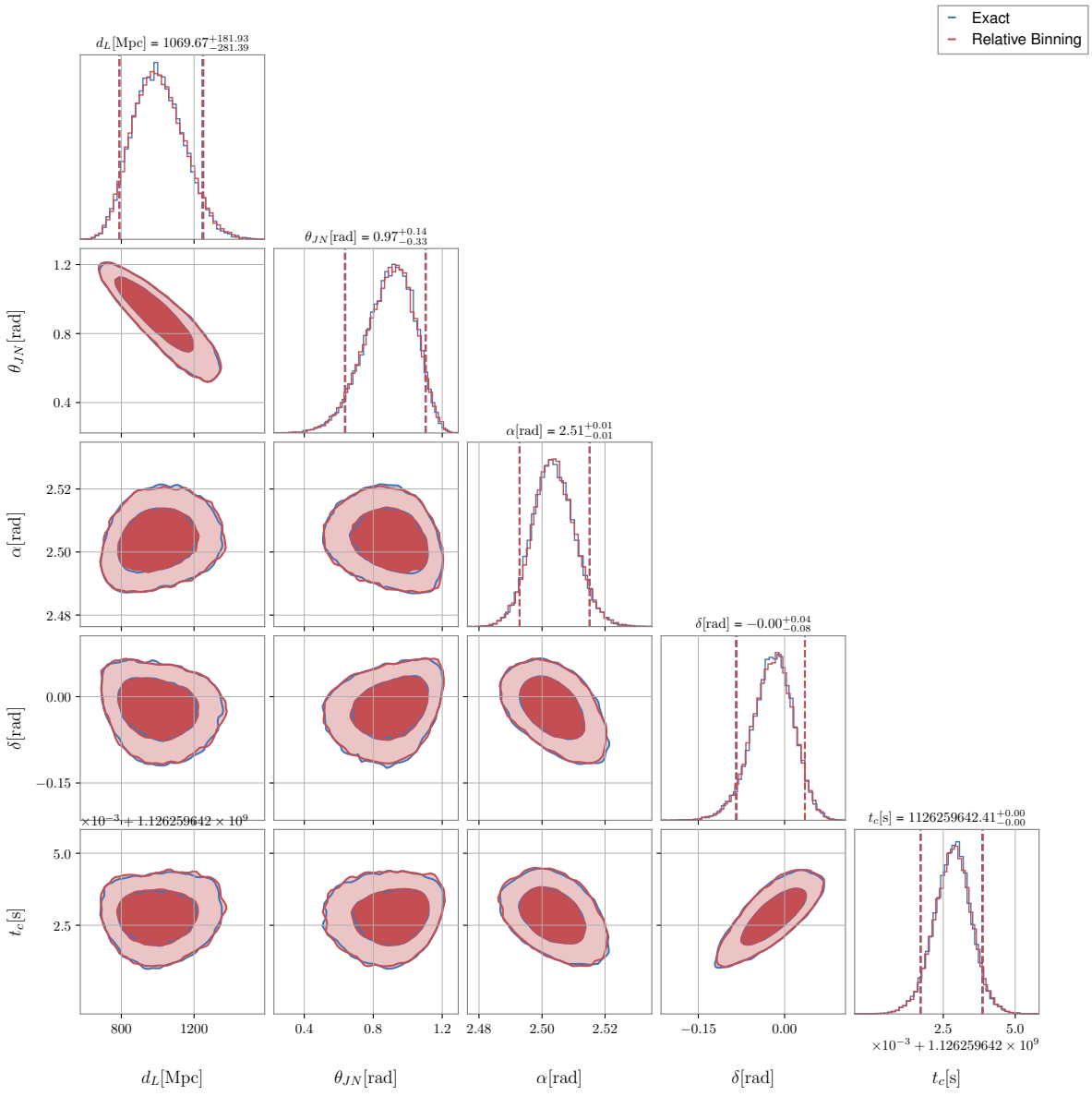

Figure 6. Corner plot comparing the extrinsic parameters estimated using relative binning (red) and exact (blue) methods for the BBH injection seen in Figure 5. The `IMRPhenomXPHM` approximant, which includes the effects of several non-quadrupole modes, was used for likelihood evaluations.

Table V. Speed-up factors for GW signals of different durations. We used `IMRPhenomPv2` and `IMRPhenomPv2_NRTidal` approximants for the BBH and BNS signals respectively.

GW Signal Type	**Duration** (s)	$\mathcal{L}$ **calc time** (ms)		**Speed-up Factor**
		Exact	**Relbin**	
BBH (GW150914-like)	4	3.967	1.245	3
XG BBH	32	55.538	1.663	33
BNS (GW170817-like)	128	275.89	1.713	161
XG BBH	1024	2069.99	1.643	1260
XG BNS	4096	9225.77	1.893	4874

future GW detections. In this work, we describe the implementation of relative binning in `Bilby`. We have

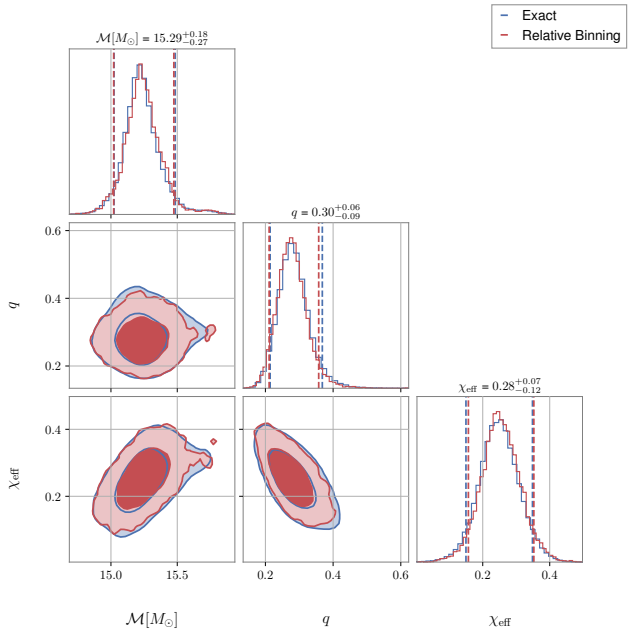

Figure 7. Corner plot showing the posterior distributions on the intrinsic parameters of GW190412 calculated using the exact likelihood and the relative binning likelihood.

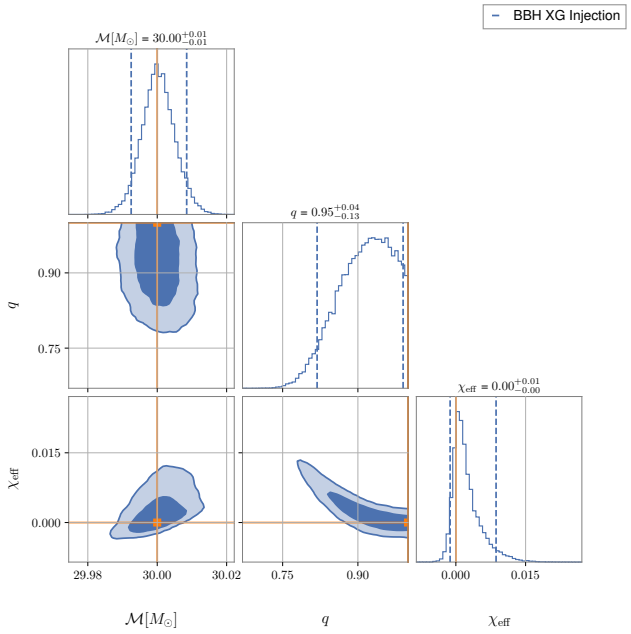

Figure 8. Corner plot showing the posterior distributions for intrinsic parameters of a BBH injection in XG ground-based network estimated using relative binning. Solid orange lines indicate the injected parameters. The Marginalized 1-dimensional histograms for each parameter are shown along the diagonal with dashed vertical lines and labels for 5% and 95% quantiles of the parameters. Off-diagonal plots show 2-dimensional joint-posterior distributions with contours corresponding to the 68% and 95% credible regions. The waveform approximant used is `IMRPhenomPv2`. See table IV for more details.

shown that our implementation is able to successfully recover parameters of GW170817 in 14 hours on a single CPU core. The sampling time will only reduce when the sampler is parallelized over multiple cores. We also showed that our implementation works well with injected sources, and also passes p-p tests. This enables large-scale injection campaigns with low mass GW signals without very high associated computational costs. Our `Bilby` implementation allows further testing and investigation of the technique and its use in the current observing run (O4) of the LVK collaboration. Additionally, `Bilby`'s user-friendly interface makes relative binning accessible to everyone.

Although we have performed validation checks by testing the accuracy of our code against the exact method for ample GW signals, more work needs to be done to assess its performance on a larger population. Such studies investigating the impact of the relative binning technique in various corners of the parameter space have been absent from the literature. We have shown that the advantage of using relative binning increases with duration of detected events. This makes it a powerful tool for parameter estimation of binary neutron star mergers and neutron star – black hole mergers in O4. The promise of relative binning for multi-messenger parameter estimations and follow-ups has already been demonstrated by [56] and [40]. As we have shown, relative binning will also prove to be immensely useful for detections with XG ground-based interferometers.

ACKNOWLEDGMENTS

We thank Ish Gupta and Ajith Parameswaran for a reading of our draft. We also thank the entire `Bilby` O4 review team for their efforts in getting this pipeline reviewed for LVK analyses, especially Gregory Ashton, Charlie Hoy, and Simon Stevenson.

This work was supported by Department of Atomic Energy, Government of India, under Project No. RTI4001. AV acknowledges support from the Natural Sciences and Engineering Research Council of Canada (NSERC) (funding reference number 568580). CT is supported by the Eric and Wendy Schmidt AI in Science Postdoctoral Fellowship, a Schmidt Futures program. AZ was supported by NSF Grants PHY-2207594 and PHY-2308833.

This research has made use of data or software obtained from the Gravitational Wave Open Science Center (gwosc.org), a service of LIGO Laboratory, the LIGO Scientific Collaboration, the Virgo Collaboration, and KAGRA [76]. LIGO Laboratory and Advanced LIGO are funded by the United States National Science Foundation (NSF) as well as the Science and Technology Facilities Council (STFC) of the United Kingdom, the Max-Planck-Society (MPS), and the State of Niedersachsen/Germany

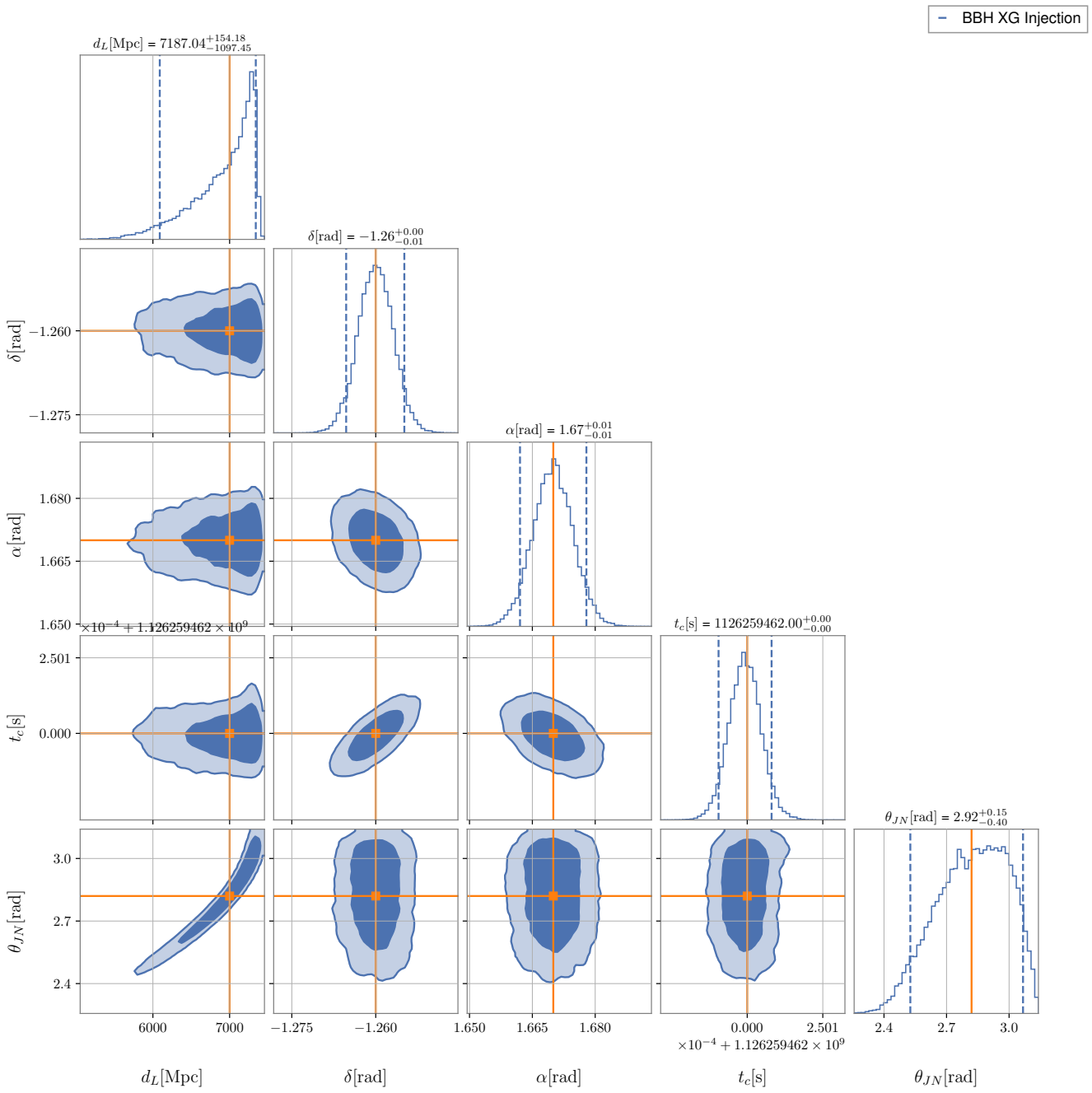

Figure 9. Corner plot for extrinsic parameters of the BBH injection from Figure 8. Solid orange lines indicate the injected parameters. The Marginalized 1-dimensional histograms for each parameter are shown along the diagonal with dashed vertical lines and labels for 5% and 95% quantiles of the parameters. Off-diagonal plots show 2-dimensional joint-posterior distributions with contours corresponding to the 68% and 95% credible regions. The waveform approximant used is `IMRPhenomPv2`.

for support of the construction of Advanced LIGO and construction and operation of the GEO600 detector. Additional support for Advanced LIGO was provided by the Australian Research Council. Virgo is funded, through the European Gravitational Observatory (EGO), by the French Centre National de Recherche Scientifique (CNRS), the Italian Istituto Nazionale di Fisica Nucleare (INFN), and the Dutch Nikhef, with contributions by institutions from Belgium, Germany, Greece, Hungary, Ireland, Japan, Monaco, Poland, Portugal, Spain. KAGRA is supported by the Ministry of Education, Culture, Sports, Science and Technology (MEXT), Japan Society for the Promotion of Science (JSPS) in Japan; National Research Foundation (NRF) and the Ministry of Science and ICT (MSIT) in

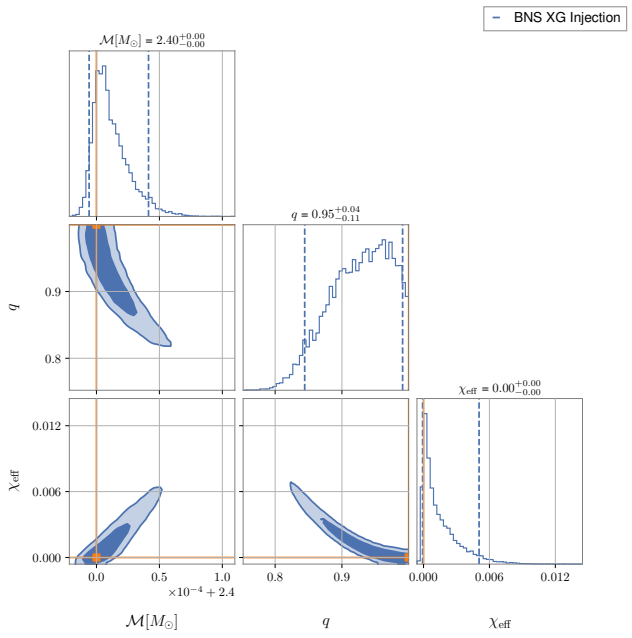

Figure 10. Corner plot showing the posterior distributions for intrinsic parameters of a BNS injection in XG ground-based network estimated using relative binning. Solid orange lines indicate the injected parameters. The Marginalized 1-dimensional histograms for each parameter are shown along the diagonal with dashed vertical lines and labels for 5% and 95% quantiles of the parameters. Off-diagonal plots show 2-dimensional joint-posterior distributions with contours corresponding to the 68% and 95% credible regions. The waveform approximant used is `IMRPhenomPv2`. See table IV for more details.

Korea; Academia Sinica (AS) and National Science and Technology Council (NSTC) in Taiwan.

This work has made use of the `numpy` [77], `scipy` [55], `matplotlib` [78], `jupyter` [79], `pandas` [80], `bilby` [38], `bilby_pipe` [39], `corner` [81], `dynesty` [57], `PESummary` [82] software packages.

Appendix A: Time Marginalization in Relative Binning

In this appendix, we demonstrate why time marginalization is not feasible for relative binning. The formula for time-marginalised likelihood [50] is

$$\log \mathcal{L}^{t}_{\rm marg} = \log \mathcal{Z}_N - \frac{1}{2}\rho^2_{\rm opt}(\tilde{\boldsymbol{\theta}}) + \log \sum_{n=0}^{N-1} e^{\kappa^2(\tilde{\boldsymbol{\theta}},n)}\pi_n \quad \text{(A1)}$$

where

$$\kappa^2(n) = 4\Delta f\ \mathfrak{Re}\Big\{\texttt{fft}_n\left(\frac{d\ \mu^*(t_0)}{S_n(f)}\right)\Big\} \quad \text{(A2)}$$

With relative binning, the computation of the $\kappa^2(n)$ array is not that straightforward. Let us consider two possible ways to do this.

- Alternative I: In table I, we saw that the waveform ratio $r(f)$ for any given waveform $\mu(\tilde{\boldsymbol{\theta}}, f)$ is only evaluated at the bin edges. But let's say we want the values of $r(f)$ over the frequency grid. One way to do this would be to interpolate the existing values of $r(f)$ using the linear-fit coefficients (which were obtained from $r(f)$ at the bin edges) as seen in eq. 1.

  $$r_{interp}(f) = r_0(\mu, \mathrm{b}) + r_1(\mu, \mathrm{b})\,(f - f_{\rm m}(\mathrm{b})) \quad \text{(A3)}$$

  Now the interpolated waveform ratio that spans the entire frequency grid can be used to compute the $\kappa^2(n)$ array as follows:

  $$\begin{aligned}\kappa^2(n) &= 4\Delta f\ \mathfrak{Re}\Big\{\texttt{fft}_n\left(\frac{d\ \mu^*(t_0)}{S_n(f)}\right)\Big\} \\ &= 4\Delta f\ \mathfrak{Re}\Big\{\texttt{fft}_n\left(\frac{d\ \mu_0^*(t_0) r^*_{\rm interp}(t_0)}{S_n(f)}\right)\Big\}\end{aligned} \quad \text{(A4)}$$

  where we have used the fact that $\mu(f) = r(f)\mu_0(f)$.

- Alternative II

  The other alternative is to modify the summary data corresponding to the matched filter. We start with eq. A2 and replicate the summary data derivations in section II A.

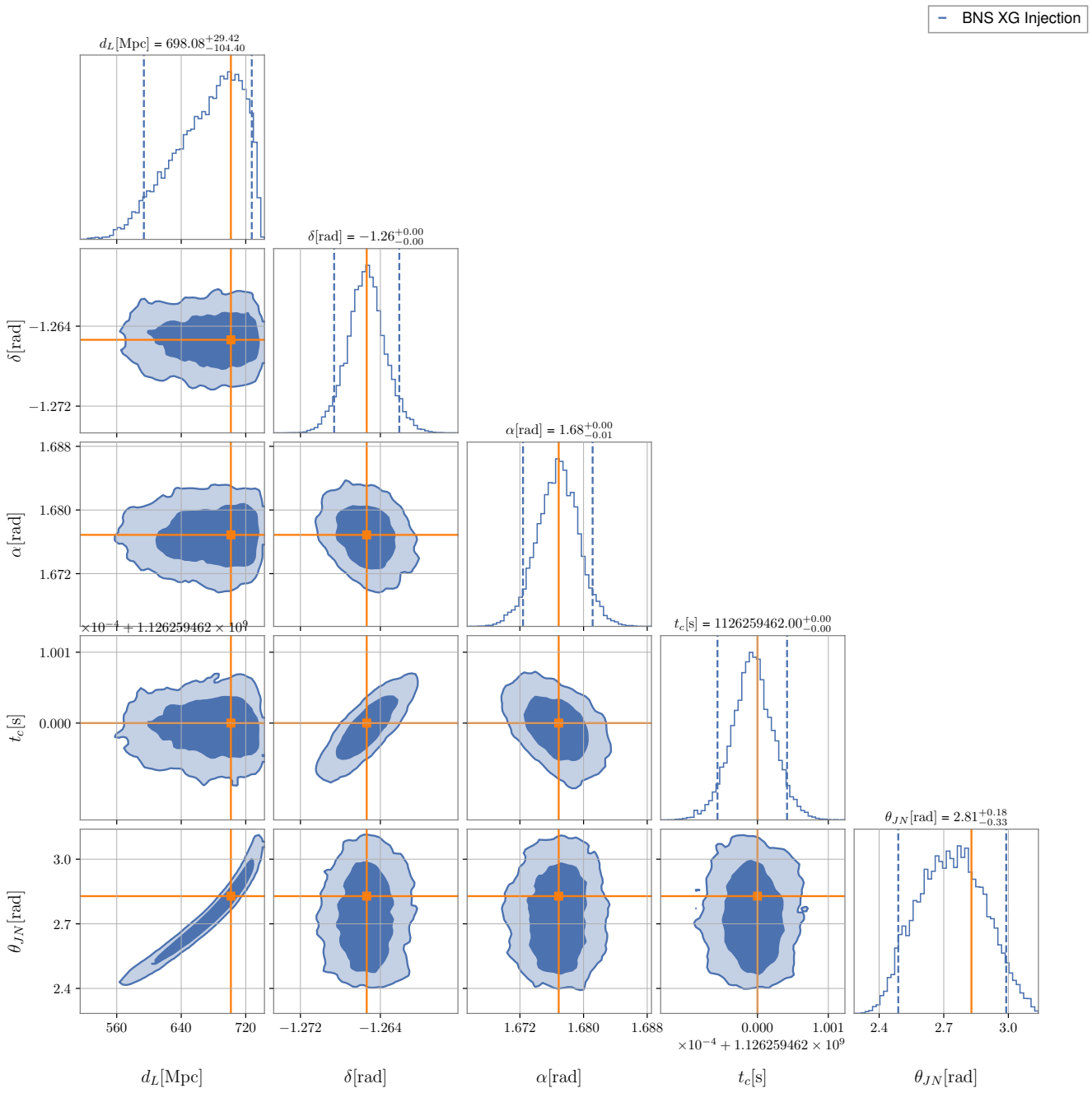

Figure 11. Corner plot for extrinsic parameters of the BNS injection from Figure 10. Solid orange lines indicate the injected parameters. The Marginalized 1-dimensional histograms for each parameter are shown along the diagonal with dashed vertical lines and labels for 5% and 95% quantiles of the parameters. Off-diagonal plots show 2-dimensional joint-posterior distributions with contours corresponding to the 68% and 95% credible regions. The waveform approximant used is `IMRPhenomPv2`.

$$\begin{aligned}
\kappa^2(n) &= 4\Delta f\ \mathfrak{Re}\sum_j^N \frac{d_j \mu_j^*(t_0)}{S_n(f_j)} e^{-2\pi i j \frac{n}{N-1}} \\
&= \mathfrak{Re}\sum_b \left(4\sum_{f_i\in b} \frac{d(f_i) r^*(f_i)\, \mu_0^*(f_i,\tilde{\boldsymbol{\theta}})}{S_n(f_i)\ T} e^{-2\pi i j \frac{n}{N}}\right) \\
&\approx \mathfrak{Re}\sum_b \left(r_0^*(\mu,\mathrm{b})\left(4\sum_{f_i\in b} \frac{d(f_i)\ \mu_0^*(f_i,\tilde{\boldsymbol{\theta}})}{S_n(f_i)\ T} e^{-2\pi i j \frac{n}{N}}\right)\right. \\
&\qquad \left. + r_1^*(\mu,\mathrm{b})\left(4\sum_{f_i\in b} \frac{d(f_i)\ \mu_0^*(f_i,\tilde{\boldsymbol{\theta}})}{S_n(f_i)\ T} (f - f_{\mathrm{m}}(\mathrm{b})) e^{-2\pi i j \frac{n}{N}}\right)\right) \\
&\approx \mathfrak{Re}\sum_{\mathrm{b}} \left(A_0^t(\mathrm{b}) r_0^*(\mu,\mathrm{b}) + A_1^t(\mathrm{b}) r_1^*(\mu,\mathrm{b})\right) \qquad \text{(A5)}
\end{aligned}$$

where
$$A_0^t(n,\mathrm{b}) = 4\sum_{f\in \mathrm{b}} \frac{d(f)\mu_0^*(f)}{S_n(f)\ T} e^{-2\pi i j \frac{n}{N}} \qquad \text{(A6)}$$

$$A_1^t(n,\mathrm{b}) = 4\sum_{f\in \mathrm{b}} \frac{d(f)\mu_0^*(f)}{S_n(f)\ T} e^{-2\pi i j \frac{n}{N}}\ (f - f_{\mathrm{m}}(\mathrm{b})) \qquad \text{(A7)}$$

We end up with modified summary data $A_0^t(n,\mathrm{b})$ and $A_1^t(n,\mathrm{b})$. Note that these terms also depend on n, the discretised coalescence time. On the other hand, $B_0(\mathrm{b})$ and $B_1(\mathrm{b})$ remain unchanged as $\rho^2_{\mathrm{opt}}(\tilde{\boldsymbol{\theta}})$ is unaffected by the coalescence time.

In alternative I, though the waveform generation time is saved, the number of complex multiplications involved goes as $\mathcal{O}(N)$, where N is the number of points in a full FFT grid. Therefore, the marginalised likelihood computation takes more time than the normal likelihood computation with relative binning in this case. Whereas in alternative II, though the two-fold time saving discussed in section II still holds, the pre-computation time is increased by $\mathcal{O}(2N)$. This is because $A_0^t(n,\mathrm{b})$ and $A_1^t(n,\mathrm{b})$ will have to be calculated at N points for each bin as $n = 0, 1, ..., N-1$. In this case, the increase in the pre-computation time is higher than the time saved by reducing the dimensionality of the parameter space by one with time marginalization. Therefore, with relative binning, marginalizing over time only slows down the parameter estimation. Nevertheless, Alternative I is included as an option for time marginalization in the `Bilby` implementation.

[1] J. Aasi *et al.* (LIGO Scientific), "Advanced LIGO," Class. Quant. Grav. **32**, 074001 (2015), arXiv:1411.4547 [gr-qc].

[2] F. Acernese *et al.* (VIRGO), "Advanced Virgo: a second-generation interferometric gravitational wave detector," Class. Quant. Grav. **32**, 024001 (2015), arXiv:1408.3978 [gr-qc].

[3] Kentaro Somiya (KAGRA), "Detector configuration of KAGRA: The Japanese cryogenic gravitational-wave detector," Class. Quant. Grav. **29**, 124007 (2012), arXiv:1111.7185 [gr-qc].

[4] Yoichi Aso, Yuta Michimura, Kentaro Somiya, Masaki Ando, Osamu Miyakawa, Takanori Sekiguchi, Daisuke Tatsumi, and Hiroaki Yamamoto (KAGRA), "Interferometer design of the KAGRA gravitational wave detector," Phys. Rev. D **88**, 043007 (2013), arXiv:1306.6747 [gr-qc].

[5] T. Akutsu *et al.* (KAGRA), "Overview of KAGRA: Detector design and construction history," PTEP **2021**, 05A101 (2021), arXiv:2005.05574 [physics.ins-det].

[6] B. P. Abbott *et al.*, "Multi-messenger Observations of a Binary Neutron Star Merger," Astrophys. J. Lett. **848**, L12 (2017), arXiv:1710.05833 [astro-ph.HE].

[7] B. P. Abbott *et al.* (LIGO Scientific, Virgo), "Properties of the binary neutron star merger GW170817," Phys. Rev. X **9**, 011001 (2019), arXiv:1805.11579 [gr-qc].

[8] B. P. Abbott *et al.* (LIGO Scientific, Virgo), "GW170817: Measurements of neutron star radii and equation of state," Phys. Rev. Lett. **121**, 161101 (2018), arXiv:1805.11581 [gr-qc].

[9] R. Abbott *et al.* (LIGO Scientific, Virgo), "Population Properties of Compact Objects from the Second LIGO-Virgo Gravitational-Wave Transient Catalog," Astrophys. J. Lett. **913**, L7 (2021), arXiv:2010.14533 [astro-ph.HE].

[10] R. Abbott *et al.* (KAGRA, VIRGO, LIGO Scientific), "Population of Merging Compact Binaries Inferred Using Gravitational Waves through GWTC-3," Phys. Rev. X **13**, 011048 (2023), arXiv:2111.03634 [astro-ph.HE].

[11] R. Abbott *et al.* (LIGO Scientific, Virgo), "Tests of general relativity with binary black holes from the second LIGO-

Virgo gravitational-wave transient catalog," Phys. Rev. D **103**, 122002 (2021), arXiv:2010.14529 [gr-qc].
[12] R. Abbott *et al.* (LIGO Scientific, VIRGO, KAGRA), "Tests of General Relativity with GWTC-3," (2021), arXiv:2112.06861 [gr-qc].
[13] R. Abbott *et al.* (LIGO Scientific, Virgo, KAGRA), "Constraints on the Cosmic Expansion History from GWTC–3," Astrophys. J. **949**, 76 (2023), arXiv:2111.03604 [astro-ph.CO].
[14] John Miller, Lisa Barsotti, Salvatore Vitale, Peter Fritschel, Matthew Evans, and Daniel Sigg, "Prospects for doubling the range of Advanced LIGO," Phys. Rev. D **91**, 062005 (2015), arXiv:1410.5882 [gr-qc].
[15] B. P. Abbott *et al.* (KAGRA, LIGO Scientific, Virgo, VIRGO), "Prospects for observing and localizing gravitational-wave transients with Advanced LIGO, Advanced Virgo and KAGRA," Living Rev. Rel. **21**, 3 (2018), arXiv:1304.0670 [gr-qc].
[16] Benjamin P Abbott *et al.* (LIGO Scientific), "Exploring the Sensitivity of Next Generation Gravitational Wave Detectors," Class. Quant. Grav. **34**, 044001 (2017), arXiv:1607.08697 [astro-ph.IM].
[17] M. Punturo *et al.*, "The Einstein Telescope: A third-generation gravitational wave observatory," Class. Quant. Grav. **27**, 194002 (2010).
[18] Priscilla Canizares, Scott E. Field, Jonathan Gair, Vivien Raymond, Rory Smith, and Manuel Tiglio, "Accelerated gravitational-wave parameter estimation with reduced order modeling," Phys. Rev. Lett. **114**, 071104 (2015), arXiv:1404.6284 [gr-qc].
[19] Rory Smith, Scott E. Field, Kent Blackburn, Carl-Johan Haster, Michael Pürrer, Vivien Raymond, and Patricia Schmidt, "Fast and accurate inference on gravitational waves from precessing compact binaries," Phys. Rev. D **94**, 044031 (2016), arXiv:1604.08253 [gr-qc].
[20] Soichiro Morisaki and Vivien Raymond, "Rapid Parameter Estimation of Gravitational Waves from Binary Neutron Star Coalescence using Focused Reduced Order Quadrature," Phys. Rev. D **102**, 104020 (2020), arXiv:2007.09108 [gr-qc].
[21] Soichiro Morisaki, Rory Smith, Leo Tsukada, Surabhi Sachdev, Simon Stevenson, Colm Talbot, and Aaron Zimmerman, "Rapid localization and inference on compact binary coalescences with the Advanced LIGO-Virgo-KAGRA gravitational-wave detector network," (2023), arXiv:2307.13380 [gr-qc].
[22] Serena Vinciguerra, John Veitch, and Ilya Mandel, "Accelerating gravitational wave parameter estimation with multi-band template interpolation," Class. Quant. Grav. **34**, 115006 (2017), arXiv:1703.02062 [gr-qc].
[23] Soichiro Morisaki, "Accelerating parameter estimation of gravitational waves from compact binary coalescence using adaptive frequency resolutions," Phys. Rev. D **104**, 044062 (2021), arXiv:2104.07813 [gr-qc].
[24] Lalit Pathak, Amit Reza, and Anand S. Sengupta, "Fast likelihood evaluation using meshfree approximations for reconstructing compact binary sources," Phys. Rev. D **108**, 064055 (2023), arXiv:2210.02706 [gr-qc].
[25] Lalit Pathak, Sanket Munishwar, Amit Reza, and Anand S. Sengupta, "Prompt sky localization of compact binary sources using meshfree approximation," (2023), arXiv:2309.07012 [gr-qc].
[26] C. Pankow, P. Brady, E. Ochsner, and R. O'Shaughnessy, "Novel scheme for rapid parallel parameter estimation of gravitational waves from compact binary coalescences," Phys. Rev. D **92**, 023002 (2015), arXiv:1502.04370 [gr-qc].
[27] Jacob Lange, Richard O'Shaughnessy, and Monica Rizzo, "Rapid and accurate parameter inference for coalescing, precessing compact binaries," (2018), arXiv:1805.10457 [gr-qc].
[28] Rory J. E. Smith, Gregory Ashton, Avi Vajpeyi, and Colm Talbot, "Massively parallel Bayesian inference for transient gravitational-wave astronomy," Mon. Not. Roy. Astron. Soc. **498**, 4492–4502 (2020), arXiv:1909.11873 [gr-qc].
[29] Colm Talbot, Rory Smith, Eric Thrane, and Gregory B. Poole, "Parallelized Inference for Gravitational-Wave Astronomy," Phys. Rev. D **100**, 043030 (2019), arXiv:1904.02863 [astro-ph.IM].
[30] Vaibhav Tiwari, Charlie Hoy, Stephen Fairhurst, and Duncan MacLeod, "Fast non-Markovian sampler for estimating gravitational-wave posteriors," Phys. Rev. D **108**, 023001 (2023), arXiv:2303.01463 [astro-ph.HE].
[31] Michael J. Williams, John Veitch, and Chris Messenger, "Nested sampling with normalizing flows for gravitational-wave inference," Phys. Rev. D **103**, 103006 (2021), arXiv:2102.11056 [gr-qc].
[32] Stephen R. Green, Christine Simpson, and Jonathan Gair, "Gravitational-wave parameter estimation with autoregressive neural network flows," Phys. Rev. D **102**, 104057 (2020), arXiv:2002.07656 [astro-ph.IM].
[33] Thomas D. P. Edwards, Kaze W. K. Wong, Kelvin K. H. Lam, Adam Coogan, Daniel Foreman-Mackey, Maximiliano Isi, and Aaron Zimmerman, "ripple: Differentiable and Hardware-Accelerated Waveforms for Gravitational Wave Data Analysis," (2023), arXiv:2302.05329 [astro-ph.IM].
[34] Kaze W. K. Wong, Maximiliano Isi, and Thomas D. P. Edwards, "Fast Gravitational-wave Parameter Estimation without Compromises," Astrophys. J. **958**, 129 (2023), arXiv:2302.05333 [astro-ph.IM].
[35] Neil J. Cornish, "Fast Fisher Matrices and Lazy Likelihoods," (2010), arXiv:1007.4820 [gr-qc].
[36] Barak Zackay, Liang Dai, and Tejaswi Venumadhav, "Relative Binning and Fast Likelihood Evaluation for Gravitational Wave Parameter Estimation," (2018), arXiv:1806.08792 [astro-ph.IM].
[37] Neil J. Cornish, "Heterodyned likelihood for rapid gravitational wave parameter inference," Physical Review D **104**, 104054 (2021).
[38] Gregory Ashton *et al.*, "BILBY: A user-friendly Bayesian inference library for gravitational-wave astronomy," Astrophys. J. Suppl. **241**, 27 (2019), arXiv:1811.02042 [astro-ph.IM].
[39] I. M. Romero-Shaw *et al.*, "Bayesian inference for compact binary coalescences with bilby: validation and application to the first LIGO–Virgo gravitational-wave transient catalogue," Mon. Not. Roy. Astron. Soc. **499**, 3295–3319 (2020), arXiv:2006.00714 [astro-ph.IM].
[40] Daniel Finstad and Duncan A. Brown, "Fast Parameter Estimation of Binary Mergers for Multimessenger Follow-up," Astrophys. J. Lett. **905**, L9 (2020), arXiv:2009.13759 [astro-ph.IM].
[41] Javier Roulet, Seth Olsen, Jonathan Mushkin, Tousif Islam, Tejaswi Venumadhav, Barak Zackay, and Matias Zaldarriaga, "Removing degeneracy and multimodality in gravitational wave source parameters," Phys. Rev. D **106**, 123015 (2022), arXiv:2207.03508 [gr-qc].

[42] Harsh Narola, Justin Janquart, Quirijn Meijer, K. Haris, and Chris Van Den Broeck, "Relative binning for complete gravitational-wave parameter estimation with higher-order modes and precession, and applications to lensing and third-generation detectors," (2023), arXiv:2308.12140 [gr-qc].

[43] Nathaniel Leslie, Liang Dai, and Geraint Pratten, "Mode-by-mode relative binning: Fast likelihood estimation for gravitational waveforms with spin-orbit precession and multiple harmonics," Phys. Rev. D **104**, 123030 (2021), arXiv:2109.09872 [astro-ph.IM].

[44] Tousif Islam, Javier Roulet, and Tejaswi Venumadhav, "Factorized Parameter Estimation for Real-Time Gravitational Wave Inference," (2022), arXiv:2210.16278 [gr-qc].

[45] Bikram Keshari Pradhan, Aditya Vijaykumar, and Debarati Chatterjee, "Impact of updated multipole Love numbers and f-Love universal relations in the context of binary neutron stars," Phys. Rev. D **107**, 023010 (2023), arXiv:2210.09425 [astro-ph.HE].

[46] Aditya Vijaykumar, Avinash Tiwari, Shasvath J. Kapadia, K. G. Arun, and Parameswaran Ajith, "Waltzing Binaries: Probing the Line-of-sight Acceleration of Merging Compact Objects with Gravitational Waves," Astrophys. J. **954**, 105 (2023), arXiv:2302.09651 [astro-ph.HE].

[47] Noah E. Wolfe, Salvatore Vitale, and Colm Talbot, "Too small to fail: characterizing sub-solar mass black hole mergers with gravitational waves," JCAP **11**, 039 (2023), arXiv:2305.19907 [astro-ph.HE].

[48] Nikhil Sarin *et al.*, "Redback: A Bayesian inference software package for electromagnetic transients," (2023), arXiv:2308.12806 [astro-ph.HE].

[49] Aviral Prakash, Ish Gupta, Matteo Breschi, Rahul Kashyap, David Radice, Sebastiano Bernuzzi, Domenico Logoteta, and B. S. Sathyaprakash, "Detectability of QCD phase transitions in binary neutron star mergers: Bayesian inference with the next generation gravitational wave detectors," (2023), arXiv:2310.06025 [gr-qc].

[50] Eric Thrane and Colm Talbot, "An introduction to Bayesian inference in gravitational-wave astronomy: Parameter estimation, model selection, and hierarchical models," Publications of the Astronomical Society of Australia **36** (2019), 10.1017/pasa.2019.2.

[51] J. Veitch *et al.*, "Parameter estimation for compact binaries with ground-based gravitational-wave observations using the LALInference software library," Physical Review D - Particles, Fields, Gravitation and Cosmology **91**, 1–25 (2015).

[52] Luc Blanchet, "Gravitational Radiation from Post-Newtonian Sources and Inspiralling Compact Binaries," Living Rev. Rel. **17**, 2 (2014), arXiv:1310.1528 [gr-qc].

[53] Liang Dai, Tejaswi Venumadhav, and Barak Zackay, "Parameter Estimation for GW170817 using Relative Binning," (2018), arXiv:1806.08793 [gr-qc].

[54] Alessandra Buonanno, Bala Iyer, Evan Ochsner, Yi Pan, and B. S. Sathyaprakash, "Comparison of post-Newtonian templates for compact binary inspiral signals in gravitational-wave detectors," Phys. Rev. D **80**, 084043 (2009), arXiv:0907.0700 [gr-qc].

[55] Pauli Virtanen, Ralf Gommers, Travis E. Oliphant, Matt Haberland, Tyler Reddy, David Cournapeau, Evgeni Burovski, Pearu Peterson, Warren Weckesser, Jonathan Bright, Stéfan J. van der Walt, Matthew Brett, Joshua Wilson, K. Jarrod Millman, Nikolay Mayorov, Andrew R. J. Nelson, Eric Jones, Robert Kern, Eric Larson, C. J. Carey, İlhan Polat, Yu Feng, Eric W. Moore, Jake VanderPlas, Denis Laxalde, Josef Perktold, Robert Cimrman, Ian Henriksen, E. A. Quintero, Charles R. Harris, Anne M. Archibald, Antônio H. Ribeiro, Fabian Pedregosa, Paul van Mulbregt, and SciPy 1. 0 Contributors, "SciPy 1.0: fundamental algorithms for scientific computing in Python," Nature Methods **17**, 261–272 (2020), arXiv:1907.10121 [cs.MS].

[56] Geert Raaijmakers *et al.*, "The Challenges Ahead for Multimessenger Analyses of Gravitational Waves and Kilonova: A Case Study on GW190425," Astrophys. J. **922**, 269 (2021), arXiv:2102.11569 [astro-ph.HE].

[57] Joshua S. Speagle, "dynesty: a dynamic nested sampling package for estimating Bayesian posteriors and evidences," Mon. Not. Roy. Astron. Soc. **493**, 3132–3158 (2020), arXiv:1904.02180 [astro-ph.IM].

[58] B. P. Abbott *et al.* (LIGO Scientific, Virgo), "GW170817: Observation of Gravitational Waves from a Binary Neutron Star Inspiral," Phys. Rev. Lett. **119**, 161101 (2017), arXiv:1710.05832 [gr-qc].

[59] Tim Dietrich *et al.*, "Matter imprints in waveform models for neutron star binaries: Tidal and self-spin effects," Physical Review D **99**, 1–21 (2019).

[60] B. P. Abbott *et al.* (LIGO Scientific, Virgo), "GWTC-1: A Gravitational-Wave Transient Catalog of Compact Binary Mergers Observed by LIGO and Virgo during the First and Second Observing Runs," Phys. Rev. X **9**, 031040 (2019), arXiv:1811.12907 [astro-ph.HE].

[61] B. P. Abbott *et al.*, "GWTC-1: A Gravitational-Wave Transient Catalog of Compact Binary Mergers Observed by LIGO and Virgo during the First and Second Observing Runs," Physical Review X **9** (2018), 10.1103/PhysRevX.9.031040.

[62] J. Lin, "Divergence measures based on the Shannon entropy," IEEE Trans. Info. Theor. **37**, 145–151 (1991).

[63] Sebastian Khan, Katerina Chatziioannou, Mark Hannam, and Frank Ohme, "Phenomenological model for the gravitational-wave signal from precessing binary black holes with two-spin effects," Phys. Rev. D **100**, 024059 (2019), arXiv:1809.10113 [gr-qc].

[64] Andrew Gelman Samantha R Cook and Donald B Rubin, "Validation of software for bayesian models using posterior quantiles," Journal of Computational and Graphical Statistics **15**, 675–692 (2006).

[65] B. S. Sathyaprakash and Bernard F. Schutz, "Physics, astrophysics and cosmology with gravitational waves," Living Reviews in Relativity **12**, 1–140 (2009).

[66] Vijay Varma, Parameswaran Ajith, Sascha Husa, Juan Calderon Bustillo, Mark Hannam, and Michael Pürrer, "Gravitational-wave observations of binary black holes: Effect of nonquadrupole modes," Phys. Rev. D **90**, 124004 (2014), arXiv:1409.2349 [gr-qc].

[67] Maite Mateu-Lucena, Sascha Husa, Marta Colleoni, Héctor Estellés, Cecilio García-Quirós, David Keitel, Maria de Lluc Planas, and Antoni Ramos-Buades, "Parameter estimation with the current generation of phenomenological waveform models applied to the black hole mergers of GWTC-1," Mon. Not. Roy. Astron. Soc. **517**, 2403–2425 (2022), arXiv:2105.05960 [gr-qc].

[68] Geraint Pratten *et al.*, "Computationally efficient models for the dominant and subdominant harmonic modes of precessing binary black holes," Phys. Rev. D **103**, 104056 (2021), arXiv:2004.06503 [gr-qc].

[69] R. Abbott *et al.* (LIGO Scientific, Virgo), "GW190412:

Observation of a Binary-Black-Hole Coalescence with Asymmetric Masses," Phys. Rev. D **102**, 043015 (2020), arXiv:2004.08342 [astro-ph.HE].

[70] R. Abbott *et al.* (LIGO Scientific, VIRGO), "GWTC-2.1: Deep Extended Catalog of Compact Binary Coalescences Observed by LIGO and Virgo During the First Half of the Third Observing Run," (2021), arXiv:2108.01045 [gr-qc].

[71] LIGO Scientific Collaboration and Virgo Collaboration, "GWTC-2.1: Deep Extended Catalog of Compact Binary Coalescences Observed by LIGO and Virgo During the First Half of the Third Observing Run - Parameter Estimation Data Release," (2022), 10.5281/zenodo.6513631.

[72] Michael Pürrer and Carl-Johan Haster, "Gravitational waveform accuracy requirements for future ground-based detectors," Physical Review Research **2**, 1–26 (2020).

[73] Ssohrab Borhanian and B. S. Sathyaprakash, "Listening to the Universe with Next Generation Ground-Based Gravitational-Wave Detectors," (2022), arXiv:2202.11048 [gr-qc].

[74] Ish Gupta *et al.*, "Characterizing Gravitational Wave Detector Networks: From $A^\sharp$ to Cosmic Explorer," (2023), arXiv:2307.10421 [gr-qc].

[75] Marica Branchesi *et al.*, "Science with the Einstein Telescope: a comparison of different designs," JCAP **07**, 068 (2023), arXiv:2303.15923 [gr-qc].

[76] Rich Abbott *et al.* (LIGO Scientific, Virgo), "Open data from the first and second observing runs of Advanced LIGO and Advanced Virgo," SoftwareX **13**, 100658 (2021), arXiv:1912.11716 [gr-qc].

[77] Charles R. Harris, K. Jarrod Millman, Stéfan J. van der Walt, Ralf Gommers, Pauli Virtanen, David Cournapeau, Eric Wieser, Julian Taylor, Sebastian Berg, Nathaniel J. Smith, Robert Kern, Matti Picus, Stephan Hoyer, Marten H. van Kerkwijk, Matthew Brett, Allan Haldane, Jaime Fernández del Río, Mark Wiebe, Pearu Peterson, Pierre Gérard-Marchant, Kevin Sheppard, Tyler Reddy, Warren Weckesser, Hameer Abbasi, Christoph Gohlke, and Travis E. Oliphant, "Array programming with NumPy," Nature (London) **585**, 357–362 (2020), arXiv:2006.10256 [cs.MS].

[78] John D. Hunter, "Matplotlib: A 2D Graphics Environment," Computing in Science and Engineering **9**, 90–95 (2007).

[79] Thomas Kluyver, Benjain Ragan-Kelley, Fernando Pérez, Brian Granger, Matthias Bussonnier, Jonathan Frederic, Kyle Kelley, Jessica Hamrick, Jason Grout, Sylvain Corlay, Paul Ivanov, Damián Avila, Safia Abdalla, Carol Willing, and Jupyter Development Team, "Jupyter Notebooks—a publishing format for reproducible computational workflows," in *IOS Press* (IOS Press, 2016) pp. 87–90.

[80] Wes McKinney, "Data Structures for Statistical Computing in Python," in *Proceedings of the 9th Python in Science Conference*, edited by Stéfan van der Walt and Jarrod Millman (2010) pp. 56 – 61.

[81] Daniel Foreman-Mackey, "corner.py: Scatterplot matrices in python," The Journal of Open Source Software **1**, 24 (2016).

[82] Charlie Hoy and Vivien Raymond, "PESummary: the code agnostic Parameter Estimation Summary page builder," SoftwareX **15**, 100765 (2021), arXiv:2006.06639 [astro-ph.IM].